Bioelectrochemistry 138 (2021) 107730

Contents lists available at ScienceDirect

Bioelectrochemistry

journal homepage: www.elsevier.com/locate/bioelechem

Electrochemiluminescent biosensor for ultrasensitive detection of lymphoma at the early stage using CD20 markers as B cell-specific antigens

Farnaz Fazlali [a], Pegah Hashemi [a], Seyyed Mehdi Khoshfetrat [b], Raheleh Halabian [c], Behzad Baradaran [d], Mohammad Johari-Ahar [e,f], Pari Karami [e,f], Ali Hajian [g], Hasan Bagheri [h,*]

[a] Research and Development Department, Farin Behbood Tashkhis LTD, Tehran, Iran
[b] Chemistry Department, Faculty of Science, Ayatollah Boroujerdi University, Boroujerd, Iran
[c] Applied Microbiology Research Center, Systems Biology and Poising Institute, Baqiyatallah University of Medical Sciences, Tehran, Iran
[d] Immunology Research Center, Tabriz University of Medical Sciences, Tabriz, Iran
[e] Department of Medicinal Chemistry, School of Pharmacy, Ardabil University of Medical Sciences, Ardabil, Iran
[f] Biosensors and Bioelectronics Research Center (BBRC), Ardabil University of Medical Sciences, Ardabil, Iran
[g] Institute of Sensor and Actuator Systems, TU Wien, Vienna, Austria
[h] Chemical Injuries Research Center, Systems Biology and Poisonings Institute, Baqiyatallah University of Medical Sciences, Tehran, Iran

ARTICLE INFO

Article history:
Received 5 June 2020
Received in revised form 17 December 2020
Accepted 18 December 2020
Available online 28 December 2020

Keywords:
Biosensors
Electrogenerated chemiluminescence aptasensor
Early detection of lymphoma
CD20 biomarker
Cancer detection
Label-free aptasensors

ABSTRACT

Herein, by taking advantage of the special binding of an aptamer to the membrane surface of a B cell and accumulation of the positive charges of a nanocomposite, including luminol-chitosan-platinum nanoparticles (L-Cs-Pt NPs), on the negatively charge of the aptamer phosphate backbone, a sensitive, simple, selective and rapid strategy for the detection of lymphoma cells by a new label-free electrogenerated chemiluminescence (ECL) aptasensor has been introduced. With increasing concentrations of B lymphoma cells, the nanocomposite detaches from the aptamer, leading to a decrease in the ECL of a luminol and H_2O_2 system. With high loading of luminol and Pt NPs on a chitosan, together with the electrocatalytic effect of Pt NPs, enhanced sensitive detection of cancer cells with a limit of detection of 31 cells/mL was achieved. Step-by-step modification and biosensor response to cancer cells was monitored by electrochemical impedance spectroscopy (EIS), cyclic voltammetry (CV), and ECL. The aptasensor exhibited excellent specificity for lymphoma cells *vs* breast cancer (MCF-7) and human embryonic kidney (HEK293) cell lines as potential interferents. Finally, the performance of the aptasensor in blood samples was assessed against a commercial flow cytometric method. Satisfactory results confirmed the applicability of the proposed biosensing platform.

© 2020 Elsevier B.V. All rights reserved.

1. Introduction

Aptamers are single-stranded sequences of RNA/DNA aptamers isolated from a random sequence library by the *"in vitro"* selection and amplification Systematic Evolution of Ligands by EXponential enrichment (SELEX) process. Sensors based on aptamers (aptasensors) have been previously investigated as analytical tools in clinical analysis. Aptasensors provide the desired fast response, portability, specificity, and sensitivity, in addition to simplicity and lower cost versus conventional methods [1]. A variety of detection methods have been coupled to analysis based on aptamers [2].

Electrogenerated chemiluminescence (ECL) is a powerful and effective analytical technique that has been applied in various fields [3]. ECL is a process to convert electrochemical energy into light. In this technique, a photon is emitted from an excited molecule (during an electron transfer reactions) at the surface of an electrode [2]. Since there is no need for a light source, ECL has a very low limit of detection. Additionally, this technique offers significant features of spatial and time resolution such that emitted light location, and sample time can be controlled [4]. ECL-based methods are attractive, as they combine the advantages of electrochemical detection and chemiluminescent techniques, such as high sensitivity, wide linear range, high specificity [5], low background signal [6], inexpensive instruments, and fast response, while most current analytical methods have drawbacks such as the necessity of specialized personnel, high cost, laborious procedures, or limited sensitivity [7]. It has become

* Corresponding author.
E-mail address: h.bagheri@bmsu.ac.ir (H. Bagheri).

https://doi.org/10.1016/j.bioelechem.2020.107730
1567-5394/© 2020 Elsevier B.V. All rights reserved.

an important and powerful tool in analytical and clinical applications on account of its versatility and simplified optical setup [8]. Luminol is a well-known luminophore that can generate strong ECL signals with H_2O_2 [3]. Metal ions are traditional catalysts in the luminol-H_2O_2 reaction [9]. The generation of reactive oxygen species from H_2O_2 can be catalyzed by certain nanoparticles (NPs). The oxidation of luminol can be greatly accelerated in the presence of a high amount of these species, leading to the amplification of the ECL signal [2]. Recently, luminol functionalized NPs, instead of solution luminol use for ECL emission, have been of high research interest due to the high luminol loading possible and the catalytic properties. Specific NPs exhibiting catalytic activity for luminol molecule ECL, with high luminol surface loading have confirmed the higher sensitivity [10]. Recently, immobilization of luminol on NPs has been used for the simultaneous genotyping of single nucleotide polymorphisms (SNPs) and electrochemical DNA biosensors. However, covalent binding only through luminol nitrogen atoms to NPs limits high loading. To address this issue, signal amplification based on graphene and a metal-organic framework (MOF) has been reported [10]. Nevertheless, a weak π-π interaction of luminol on graphene and the inaccessibility of all MOF cavities for luminophore led to limitation in trace bioanalysis. In addition, signal amplification based on the single reactive function of these carriers might not meet the requirement for the detection and quantitation of low-abundance cancer cells/disease-related biomarkers. One approach to tackle these shortcomings is to produce a high concentration of active intermediates using a co-reaction accelerator. However, separation and a large distance between the co-reaction accelerator and luminophore leads to increased overall decomposition of active intermediate and decreases the efficiency of an accelerator significantly. In the light of the demand for circumventing these disadvantages, confined multiple catalysts considerably boost the signal [11]. It was realized that the polymer-based carrier might be an intriguing candidate to improve the performance of ECL aptasensors. Polymers are interesting as matrix materials to control the growth and stabilization of particles to prevent NP aggregation [12]. Recently, remarkable attempts to synthesize nanoparticles have been made using physical and chemical methods to adjust morphology, size, shape and composition, giving controlled optical and luminescent properties. The synthesis of nanoparticles involving polymer templates is considered one of the most effective ways of achieving high levels of synthetic control during the manufacture of nanoparticles. Nanoparticles synthesized with polymers as stabilizing agents usually facilitate good control over the size and morphology. The interaction between polymers and solid particles can enhance or alter the stability of particle suspension [13]. The addition of chemical capping agents to the solution controls anisotropic growth of nanoparticles. Nanocomposites in a readily processable form can also be made with the incorporation of nanoparticles into polymers. Furthermore, polymeric matrices prevent both the oxidation and coalescence of nanoparticles and thereby help in long-term stability [14]. Polymeric stabilization is used to advantage for generating narrow size distributions of nanoparticles. A polymeric layer adsorbed on a nanoparticle surface acts as a diffusion barrier to the growth species, resulting in diffusion-restricted growth of the nanoparticle. This kind of restricted growth reduces the size distribution of the initial nuclei, which finally results in the formation of monodispersed nanoparticles [13]. Chitosan (Cs) is a natural polymer isolable from crustacean shells [15] which contains primary amines that can interact with metal ions, such as Pt, as a stabilizer by chelation, and an immobilization matrix for a large amount of luminophores; thus, Cs is interesting for the synthesis of metal NPs [12,15].

One of the most frequently occurring diseases and the second leading cause of death globally, cancer is a major global healthcare challenge [16]. In cancer, effective diagnosis and treatment at an early stage is essential [17]. Increased levels of tumor markers in the neoplastic process are associated with certain tumors. Therefore, tumor marker determination has an effective role in disease screening and diagnosis [18]. Characterization of antigen properties on the cancer cell surface is essential for targeted therapy development. CD20 is an expressed membrane protein on B lymphocytes (B cell-specific antigens) at the early stages of cell differentiation [19,20]. For the first time, Tan et al. reported the binding interaction between cancerous B cell surface-antigens and antibody-drugs using the anti-CD20 antibody Rituximab as example [19]. They reported a systematic approach for utilizing the QCM technique to quantify the apparent binding constant between Raji cells and Rituximab for in depth understanding of the binding event to facilitate understanding comprehension of the mechanisms of resistance to antibody based therapy [19]. Sensitive tests of tumor markers are important for early clinical diagnosis and achieving better patient recovery [21]. Flow cytometry is routinely used in medicine as a reference method for the immunophenotypic analysis of acute leukemia and lymphoma. The most common method used by pathologists for diagnosing lymphoma consists of tissue samples stained with hematoxylin-eosin (H&E). This task is challenging and time-consuming, mainly when the objective is to classify the lymphoma type correctly [22,23]. The most recent cancer cell detection efforts have focused on the development of biosensors with adequate sensitivity and selectivity, rapid detection, and easy operation. A biosensors has proved to be an attractive and applicable tools for non-invasive diagnosis in early lung cancer [24]. ECL is a valuable tool in life science research to study basic physiological mechanisms, for detection, discovery of causes, and to find potential cures for disease. The most common and arguably the most important, commercial application to date for ECL is its use in diagnostic assays. Currently, over 50 assays, including those for thyroid disease, tumors, as cardiac markers, in fertility therapies and analytes relevant to infectious diseases, are commercially available [25].

To the best of our knowledge, an ECL-based aptasensor for determining CD20 biomarkers on the cell surface has not been reported. Huang et. al. used a sandwich platform based on the peptide and a labled antibody for the rapid and accurate determination of Rituximab in lymphoma patient plasma [26]. Our group has recently reported developing an immunosensor using boronic acid-modified magnetic graphene nanoribbons for immobilizing anti-CD20 antibodies to detect lymphoma cells by the impedimetric method [20]. In the present report, we took advantage of the high affinity of an aptamer for the B cell membrane surface and the nanoscale proximity effect between Pt NPs and luminol confined in Cs. A sensitive, simple, selective and rapid detection of lymphoma cells by the new label-free ECL aptasensor is introduced. The amine groups on the Cs lead to Pt NP formation, and Pt NPs in the nanocomposite act as the site for luminol immobilization; the combination of these components leads to the enhancement of luminol activity. Additionally, decorating the Pt NPs as catalytic probes on the Cs surface increased specific surface area, biocompatibility and conductivity compared with CS and Pt NPs alone for chemiluminescent detection and amplified the ECL luminol signal.

With increasing concentration of cancer cells, the accumulated positive charge of L-Cs-Pt NPs on the negative phosphate backbone of aptamer decreased because of the affinity of the aptamer for the cancer cells. As a result, the ECL signal of L-Cs-Pt NPs diminished.

2. Materials and methods

2.1. Reagent and chemical

Cs, potassium chloride, potassium ferricyanide, potassium ferrocyanide, sodium hydroxide, 5-amino-2,3-dihydro-1,4-phthala zinedione (luminol), acetic acid, sodium borohydride ($NaBH_4$),

chloroplatinic acid (H_2PtCl_4), tris(2-carboxyethyl)phosphine (TCEP), 6-mercapto 1-hexanol (MCH), hydrogen peroxide solution (H_2O_2), and other used materials were purchased in analytical grade from Sigma-Aldrich. Double-distilled water was used for the preparation of aqueous solutions. Lyophilized thiolated aptamer powder was purchased from FAZA Biotech Company with the following sequences (Kd = 43 nM) [27]: 5′ to 3′: AGGAGGATAGTTCGGTGGCTGTTCAGGGTCTCCTCCT

A stock solution of the aptamer was prepared using PBS (pH 7.4) and frozen and stored at −20 °C.

Three different cell lines, including Raji cells (B lymphocyte/ Burkitt's lymphoma), MCF7 cells (breast cancer cells), and HEK293 cells (human embryonic kidney cells), were obtained from the Cell Bank of the Pasteur Institute (Tehran, Iran). DMEM and RPMI medium was from Gibco-BRL, Germany, Fetal Bovine Serum (FBS) and penicillin, streptomycin was from Sigma-Aldrich, USA.

Labelled antibodies for flow cytometry were obtained from Becton Dickinson (BD, San Jose, CA) and Dako (Carpinteria, CA): CD20 (Dako), PE-CD19 APC (Dako) and Anti-CD20 FITC (Becton Dickinson).

2.2. Apparatus

A homemade chemiluminescence detector (photomultiplier tube voltage 800 V) was used for the ECL measurements, and an Ivium potentiostat/galvanostat (Vertex, Ivium Technologies, and the Netherlands) was applied to electrochemical measurement. All electrochemical experiments were performed using a conventional three electrode system containing a working electrode: gold electrode (GE) form Compact Disk-R, an auxiliary electrode: a platinum wire, and a reference electrode: Ag/AgCl/3.0 M KCl and the data obtained were analyzed by IviumStat. The step potential (SP) method was performed to record the ECL emission of L-Cs-Pt NPs with optimise pulse potential conditions: 0.45 V, pulse period: 30 s, and pulse time: 1 s. The UV–Vis spectra were recorded using a Perkin Elmer UV/Vis Spectrometer Lambda 12 in the wavelength range of 200–800 nm. A Philips, CM30, Netherlands, was used to obtain transmission electron microscopy (TEM) images and energy-dispersive X-ray spectra (EDX) obtained by SEM-EDX, XL30, Philips, Netherlands. A flow cytometer (FC500 cytometer, Beckman-Coulter, Milan, Italy) equipped with a COULTER (Q-PREP) was utilized using routine protocols. An ELISA microplate reader (Bio-Rad, USA) was used to measure the absorbance of formazan in living cells at λ = 570 nm.

In electrochemical impedance spectroscopy (EIS) experiments, Nyquist plots were obtained a 0.1 Hz–100 kHz frequency range, applying a DC potential of 0.22 V and AC potential of 10.0 mV. All EIS experiments were performed in 10 mM PBS (pH 7.4) containing redox probe solution (5.0 mM $Fe(CN)_6^{3-/4-}$ (1:1)) and 0.10 M KCl.

For ECL measurement with the aptasensor, the aptasensor was placed in a cell containing PBS and H_2O_2 (2 mM) and the ECL signal measured. Next, the aptasensor was washed and incubated with a sample containing Raji cells for 30 min, then H_2O_2 is added to the cells and the ECL signal measured again. The difference between the ECL signal before and after incubation with Raji cells represented an analytical signal correlated with the concentration of cells in the sample. Each aptasensor was used for one assay and discarded.

2.3. Synthesis of L-Cs–Pt NPs

50 mg Cs were added to 10 mL of 1% V/V aqueous acetic acid solution (pH = 3–4) and stirred until completely dissolved. Then, 15 mL of H_2PtCl_6 (0.01 M) was added with stirring for 1 h to obtain a well-dispersed solution. In the next step, 15 mL luminol (0.01 M) was added. Finally, H_2PtCl_6 was reduced to Pt NPs by the addition of $NaBH_4$ (0.05 mL, 5%). Then, the obtained nanocomposite was separated by centrifugation and washed several times with double-distilled water. The synthesized L-Cs-Pt NPs were dispersed in PBS and stored at 4.0 °C before use.

2.4. Fabrication of the aptasensor

In this study, an archival gold reflective compact disk (CD) [4] was applied as a working electrode to fabricate the sensor. First, a piece was cut of the CD (1 cm × 1 cm) with a paper guillotine, and placed in concentrated nitric acid to remove the protective layer and expose the gold surface. The GE surface obtained was then thoroughly washed with water and electrochemically cleaned by repeat potential cycling over 0 to 1.5 V until reproducible voltammograms were obtained in sulfuric acid solution (0.5 M). Based on the literature, the gold electrode surface area was measured by following voltammograms in sulfuric acid (0.5 M) and assuming a specific charge of 386 μC cm^{-2} for gold oxide reduction [28,29]. The gold electrode surface area was determined to be 0.2 3 ± 0.02 cm^2.

In the next step, the disulfide end of the aptamer was deprotected to a thiol using TCEP (20 μL of aptamer 4 μM was added to PBS containing 5 mM TCEP and kept in darkness for 1 h). Then, 10 μL of aptamer solution was dropped on the cleaned GE and kept for 24 h. The aptamer-modified electrode was rinsed using water to remove unbound aptamer and subsequently treated with MCH (5 μL, 2 mM) for 2 h to cover the nonspecific binding sites on the surface. Finally, 10 μL of L-Cs-Pt NPs was dropped on to the surface, and after 1 h, the aptasensor were exposed to lymphoma cells. The fabrication steps of the proposed aptasensor are shown in Schematic 1.

2.5. Cell culture

The cells were expanded according to the institute protocol: the Raji cells were cultured in DMEM-high glucose, while MCF7 and HEK293 cells were cultured in RPMI. Briefly, these cell lines were cultured in 25 cm^2 cell culture flasks and grown in DMEM or RPMI mediums containing 10% FBS, 100 U/mL penicillin, and 100 μg/mL streptomycin. After two passages, the cells were suitable for experiments.

2.6. Methyl thiazole tetrazolium (MTT) assay

Various concentrations of L-Cs-Pt NPs were assessed for cytotoxicity by MTT assay over 24 h. Briefly, after cell counting, 8×10^3 Raji cells (B lymphocyte/ Burkitt's lymphoma) with 100 μL of medium were placed in each well of 96-well plates and grown overnight at 37 °C. The cells were treated with various concentrations of L-Cs-Pt NPs to study their cytotoxic effect. In parallel, control experiments were conducted without L-Cs-Pt NPs. After the incubation time, MTT-based assay was performed to evaluate the viability of the cells by following a reported protocol [30], with some modification. Briefly, the medium for the cells was removed and 10 μL of 5 mg/mL MTT with 90 μL of fresh medium (without FBS and antibiotics) was added to each well. The plated cells were incubated at 37 °C for 4 h. After the incubation period, the medium containing MTT was removed and cells incubated for another 10 min in 150 μL of 1:1 ethanol/DMSO. In living cells, the absorbance of formazan was measured at λ = 570 nm by an ELISA microplate reader. All measurements were carried out in triplicate. Cell viability was calculated as follows: % of cell viability = $([OD]_{test} - [OD]_{blank}/[OD]_{control} - [OD]_{blank}) \times 100$.

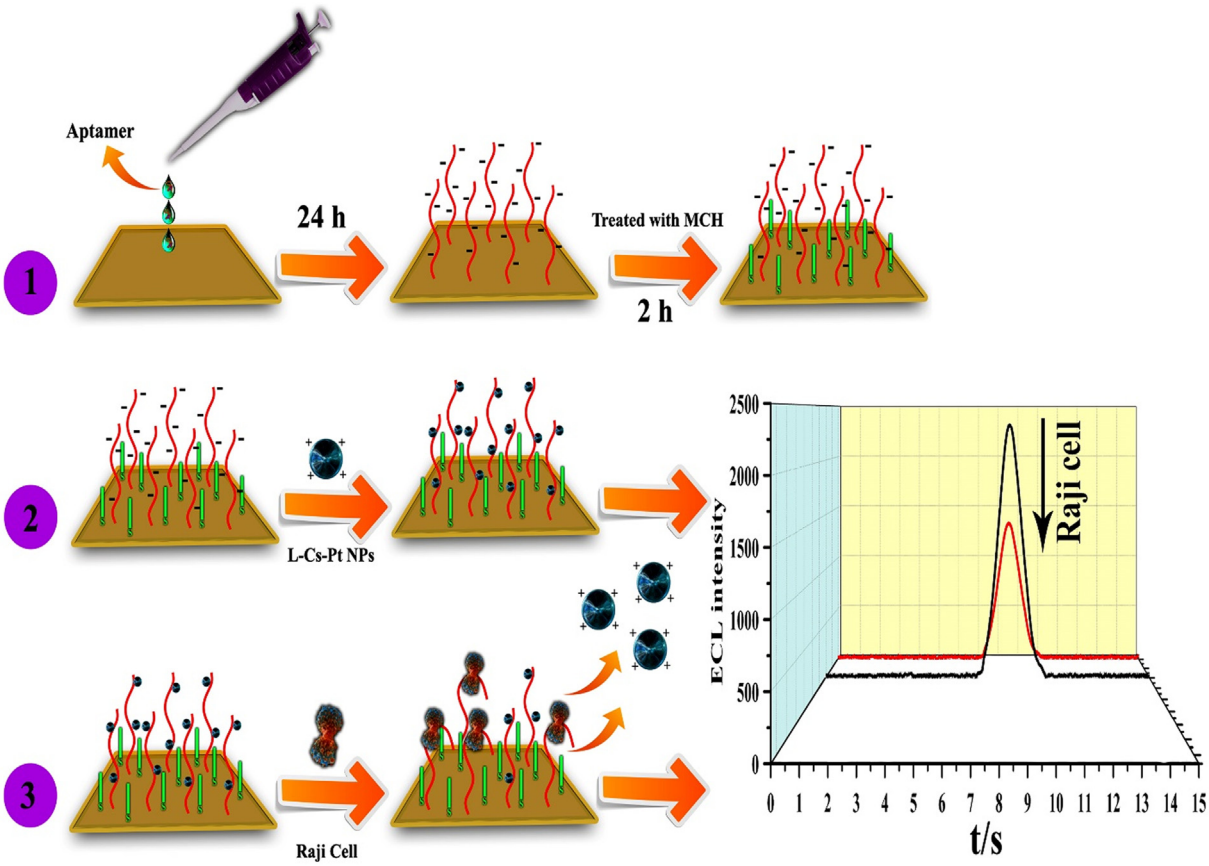

Schematic 1. Aptasensor construction process: (1) Modification of GE surface with aptamer strands and block the surface by MCH, (2) Dropping the L-Cs-Pt NPs on the modified surface electrode, (3) Incubation of the electrode surface with Raji cells.

2.7. Real sample preparation

Two samples (cancer patients) of whole human blood with coded, unattributable, information were obtained from the clinical laboratory of Baqiyatallah Al'Azam Hospital before final disposal and were used as received without further treatment.

Flow cytometry was performed using routine protocols in place at the time of diagnosis [31]. In this study, it was used for all samples with 2-color fluorescently labelled tracking antibodies. According to the manufacturer's instructions, 100 μL of whole blood or cells was mixed with 10 μL volumes of each pre-titred antibody (per test) and incubated for 20 min at 25 °C. Cells were first washed by adding 1 mL of buffer, then, lysis buffer, fixed buffer, and binding buffer were mixed in, and the cell pellet was resuspended with a suitable amount of solution. Cells were collected after separation on the Coulter. In addition, a similar numbers of cells (Raji cells) were also stained with CD20 and PE-labelled CD19 antibodies.

3. Results

3.1. Characterization of L-Cs-Pt NPs

The UV–Vis spectra of platinum, Cs, and aqueous luminol solutions, as well as L-Cs-Pt NPs, are shown in Fig. 1a. The Cs solution shows no adsorption peak. The luminol solution spectrum exhibits three distinct absorption peaks at 225, 305, and 360 nm. The shoulder band for the H_2PtCl_6 aqueous solution at approximately 270 nm disappeared after reduction to Pt NP by $NaBH_4$ and exhibited a strong absorption band at approximately 210 nm. The L-Cs-Pt NPs show the typical absorption peaks for each component, indicating that nanoparticles have been synthesized [10,32–34]. The TEM image of L-Cs-Pt NPs is shown in Fig. 1b. As shown in the image, Pt NPs were well dispersed in the Cs matrix, which suggests that the amino groups in the Cs solution played a role in Pt NP stabilization. The average diameter of the particles was observed to be approximately 12 nm. The appearance of emission lines for C, O, and N indicates that luminol and Cs were present in the nanoparticles. The demonstration of Pt in the EDX spectrum confirmed that Pt NPs were successfully produced (Fig. 1c).

3.2. Electrochemical characterization of the L-Cs-Pt NPs

Noble metal nanoparticles, such as Pt NPs, can form strongly covalent bonds to –CN, $–NH_2$, or –SH functional groups [35]. The amine groups on the Cs lead to Pt NP formation on the linear chain polymer dependent on length, and the presence of Cs causes an increase in the Pt NPs on the nanocomposite surface. Available Pt NPs in the nanocomposite act as the site for luminol immobilization, and, thus, the presence of these NPs leads to the enhancement of luminol. As shown in Fig. 2, an obvious signal was obtained with Cs, while a very weak signal was obtained without Cs. Additionally, the elimination of Pt NPs from the nanocomposite leads to a decrease in the luminol signal of L-Cs compared to L-Cs-Pt NPs. The reason may be that the luminol immobilization sites have decreased. Additionally, Pt NPs have shown catalytic activity toward luminol oxidation. On the other hand, Cs can help to increase the Pt NPs and, in the end, increase the luminol on the nanocomposite surface. The results obtained also indicated that with the elimination of Pt NPs on the nanocomposite, surface-immobilized luminol subsequently decreased.

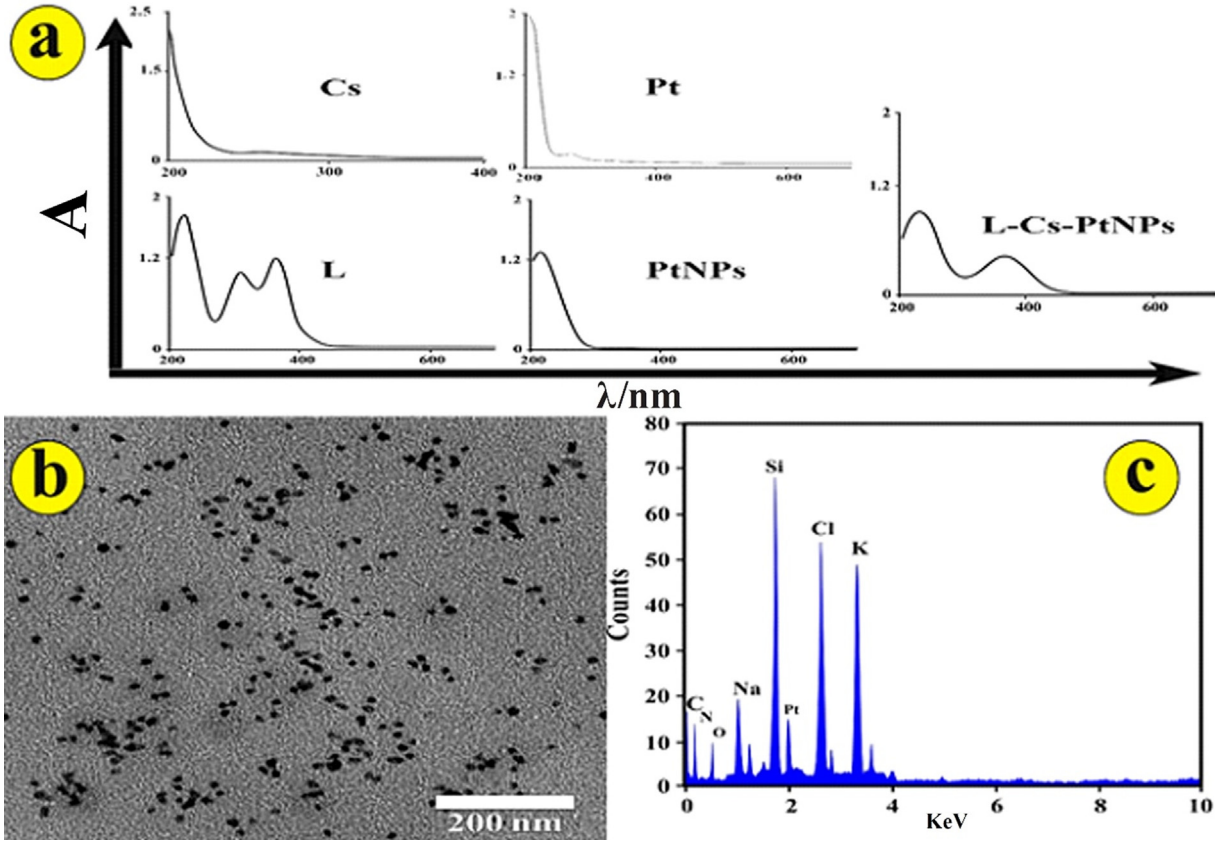

Fig. 1. Characterization of the synthesized L-Cs-Pt NPs. (a) UV–Vis spectra of platinum, Cs and luminol aqueous solution, Pt NPs and L-Cs-Pt NPs, (b) recorded TEM image and (c) EDX spectrum from L-Cs-Pt NPs.

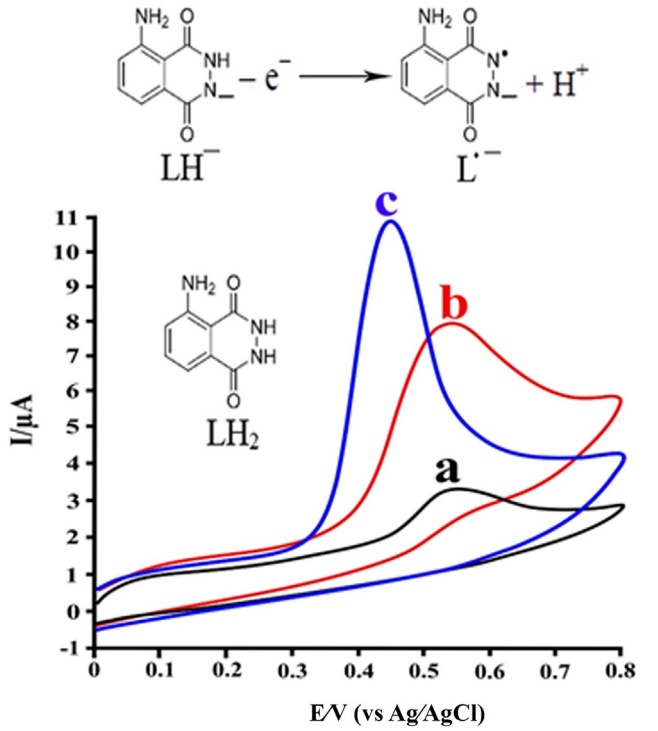

Fig. 2. Cyclic voltammograms of (a) L (0.01 M), (b) L-Cs, and (c) L-Cs-Pt NPs on the GE in PBS (0.01 M, pH = 7.4), scan rate = 100 mV s^{-1}. Inset: the suggested electrooxidation mechanism for luminol at pH = 7.4 [38,39].

The oxidation of luminol was not accompanied by a cathodic wave, which indicates that the electrode reaction is irreversible [36]. Luminol is a diprotic acid (denoted as LH_2) with pKa values of 6 and ~13, respectively. The protons from the amine moiety are relatively stable and are less acidic than the acyl-hydrazide protons on the molecule [37]. As can be seen in Fig. 2 in pH 7.4 PBS containing luminol, a small oxidation peak was noticeable at approximately 0.52 V, which could be attributed to the electro-oxidation of the luminol anion (LH^-) to a luminol radical anion ($L^{\cdot}$) according to the following reaction [38]:

$$LH^- - e^- \rightarrow L^{\cdot} + H^+ \quad (1)$$

3.3. Electrochemical characterization of the aptasensor modification steps

EIS is a suitable technique for monitoring electrode interfacial properties [39]. It is an inexpensive, powerful, rapid, and label-free alternative technology for interaction monitoring at solid/liquid interfaces and has various applications in biosensor fabrication [40]. Thus, EIS measurements have been used to study the modification of electrode surface processes. Equivalent circuits modes enable a description of the electrode/electrolyte interface [41]. A modified Randles' model [34] was used to approximate the constant phase element (CPE or Q), solution resistance (Rs), electron transfer resistance (R_{CT}), and Warburg impedance (W). In this model, the semicircle diameter represents the R_{CT} of the electrochemical reaction [34,42]. These parameter values are presented in Table 1.

The Nyquist plots of the step-by-step modification of the ECL aptasensor are shown in Fig. 3. Electrochemical impedance spectra

Table 1
Obtained Randles parameters for the fabrication steps of the proposed aptasensor.

Electrode	Rs (Ω)	R_{CT} (Ω)	W (μS)	Q	
				Y0 (μS)	n
GE	79.9	244	760	3.35	0.858
GE/Ap	78.8	1740	701	4.58	0.872
GE/Ap/MCH	84.1	2340	766	2.37	0.886
GE/Ap/MCH/L-Cs-Pt NPs	77.2	1860	667	3.99	0.861
GE/Ap/MCH/L-Cs-Pt NPs/Raji cells	83.6	3180	775	2.07	0.890

fitted to the Randles circuit and the experimental spectra are shown by dashed and dotted plots, respectively. The bare GE presented a small semicircle domain and R_{CT} (244 Ω), indicating fast electron transfer of the probe at the electrode surface. Self-assembled thiolated aptamers cause an increase in the R_{CT} value (1740 Ω) of the GE due to the development of negative charges on the surface, which in turn leads to the repulsion of negatively charged $[Fe(CN)_6]^{3-/4-}$ [4]. After blocking the electrode with MCH, a larger semicircular region was observed with the estimated corresponding R_{CT} value of 2340 Ω. After the accumulation of L-Cs-Pt NPs on the surface electrode, R_{CT} decreased to 1860 Ω, which can be attributed to facilitated electron transfer by the Pt NPs [10]. After incubating the prepared aptasensor with 1000 cells/mL of lymphoma cells, R_{CT} dramatically increased (3180 Ω), indicating that cells attached to the aptasensor surface.

The EIS data for the control experiments with Raji cells in the absence of the aptamer immobilized on the electrode surfaces, are shown in Fig. S1. In the absence of the aptamer, L-Cs-PtNPs cannot accumulate on the electrode surface and the RCT of GE/MCH/L-Cs-PtNPs does not change compared to that of GE/MCH. Furthermore, when GE/MCH/L-Cs-PtNPs are incubated with Raji cells, the RCT remains unchanged. This confirms that Raji cells are not retained on the electrode surface in the absence of the aptamer.

3.4. ECL behavior of the aptasensor

The ECL behavior of various step modifications of the aptasensor was also been studied, and the results are shown in Fig. 4A. Fig. 4A shows (curves a-c) that the bare and aptamer-modified GE and MCH have no ECL signal. When L-Cs-Pt NPs were added to the electrode surface, an ECL signal appeared (curve d of Fig. 4A), indicating that the presence of luminol on the surface electrode was due to the successful interaction of L-Cs-Pt NPs with the aptamer-modified electrode. Cs induced a positive charge on the L-Cs-Pt NPs and generated electrostatic interactions with the negatively charged aptamer phosphate backbone. However, when the aptasensor was exposed to lymphoma cells, the ECL intensity decreased (Fig. 4A curve e). This can be explained by the fact that when the cells interact with the aptamer, the negative charge on the electrode surface decreases. Thus, L-Cs-Pt NPs on the electrode surface also decreased. To identify the mechanism of the reduced signal upon cancer cell binding, after exposing the GE/Ap/MCH/L-Cs-Pt NPs to lymphoma cells, the supernatant solution was separated, and the emitted ECL signal from the L-Cs-Pt NPs was investigated. As shown in Fig. 4B, an obvious signal appeared that indicated the presence of luminol in the supernatant solution. The details of the ECL measurements supporting the release of L-Cs-Pt NP nanocomposite particles in the supernatant from the biosensor incubated with Raji cells are given in the Supporting Information (Fig. S2 and corresponding discussion). The cell concentration was measured with a hemocytometer.

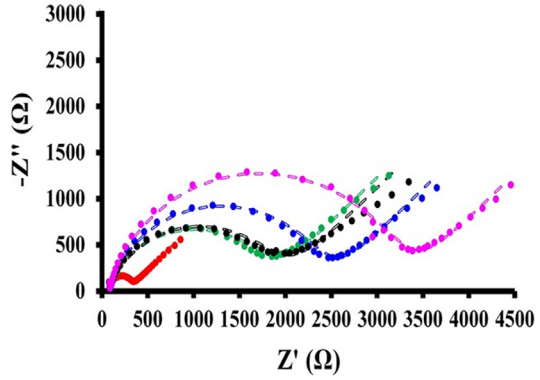

Fig. 3. Nyquist plots of the bare GE (red), GE/Ap (green), GE/Ap/MCH (blue), GE/Ap/MCH/L-Cs-Pt NPs (black), and GE/Ap/MCH/L-Cs-Pt NPs/cells (pink) in PBS containing 5 mM $[Fe(CN)_6]^{4-/3-}$ probe and KCl 0.1 M. Experimental spectra are presented as dot plots, and fitted spectra are shown as dashed plots. (For interpretation of the references to color in this figure legend, the reader is referred to the web version of this article.)

3.5. Optimization of experimental conditions

Experimental conditions such as pH, H_2O_2 concentration, and applied potential significantly affect aptasensor ECL behavior. The ECL signals from GE/Ap/MCH/L-Cs-Pt NPs were monitored at pH values from 6 to 11, and the performance of the aptasensor was investigated. The ECL intensity increased with an increase in pH over the range from 6 to 10 and then decreased in the range of 10–11 (see Fig. 5a).

The surface of the Cs hydrogel may be neutral, or positively, or negatively charged depending on the solution pH that is equal, below or above PZC [43]. The Cs hydrogel PZC is approximately 10 [43,44]. Since the L-Cs-Pt NPs at pH < 10 were positively charged, the maximum electrostatic interaction between them and immobilized aptamers on the surface was obtained, and the loading of luminol on the surface electrode at a maximum. Thus, the ECL signal was increased. At pH > 10, the L-Cs-Pt NPs were negatively charged, and the ECL signal decreased due to repulsion between the nanocomposite and aptamers. According to these results and due to the better performance and well-maintained cancer cell biological stability [45], the physiological pH was selected as the optimized pH value.

Luminol ECL at different concentrations of H_2O_2, in the range of 0.1–10 mM, was investigated. The results are shown in Fig. 5b, indicating that the ECL signal increased with increasing H_2O_2 concentration. The signal reached maximum intensity in 2 mM hydrogen peroxide and then was relatively constant.

For aptasensor preparation, potential exhibited a significant effect on ECL sensor behavior. Thus, the effect of different potentials in the range of 0–0.8 V was studied. As shown in Fig. 5c, the ECL intensities increase over the range of 0–0.45 V and decrease by a further increase in potential. At high potential, oxygen bubble formation occurs due to background reactions (such as initiated by H_2O_2 and water oxidation) that can interfere with the luminol ECL signal [10].

The PZC of the L-Cs-Pt NPs was determined in 0.01 M $NaNO_3$ solution at 20 °C. A given volume (30 mL) of 0.01 M $NaNO_3$ solution was taken and mixed with 30 mg of NPs. The pH values of the solutions were adjusted to 5–12 using solutions of HNO_3 and NaOH. The initial pH of the solution was recorded, and each flask was covered with parafilm and shaken for 24 h. The final pH values of the solutions were recorded, and the difference between initial and final pH (the so-called ΔpH) was plotted against the initial pH values. The PZC values were calculated from ΔpH versus pH plots at

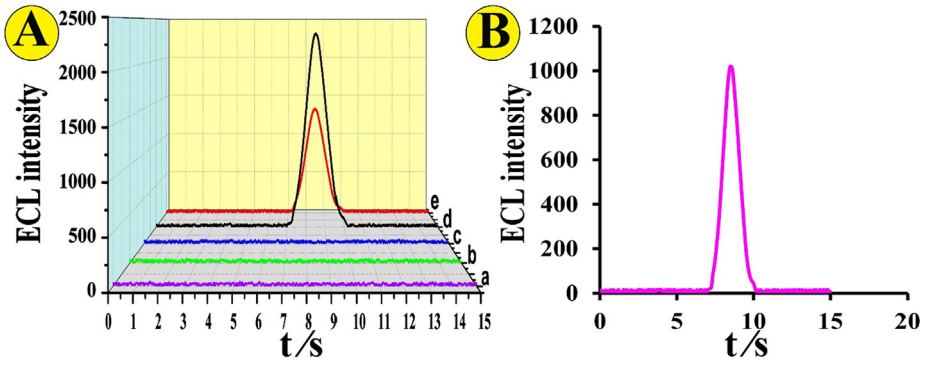

Fig. 4. (A) ECL profiles of the aptasensor in various modification steps, (a) bare GE, (b) GE/Ap, (c) GE/Ap/MCH, (d) GE/Ap/MCH/L-Cs-Pt NPs, and (e) GE/Ap/MCH/L-Cs-Pt NPs/Raji cells ($C_{Raji\ cells}$ = 1000 cells/mL) measured in PBS (pH = 7.4) containing 2 mM H_2O_2. Signals were recorded by a photomultiplier tube (PMT) detector at 800 mV. (B) ECL intensity of the supernatant solution of GE/Ap/MCH/L-Cs-Pt NPs/Raji cells ($C_{Raji\ cells}$ = 1000 cells/mL).

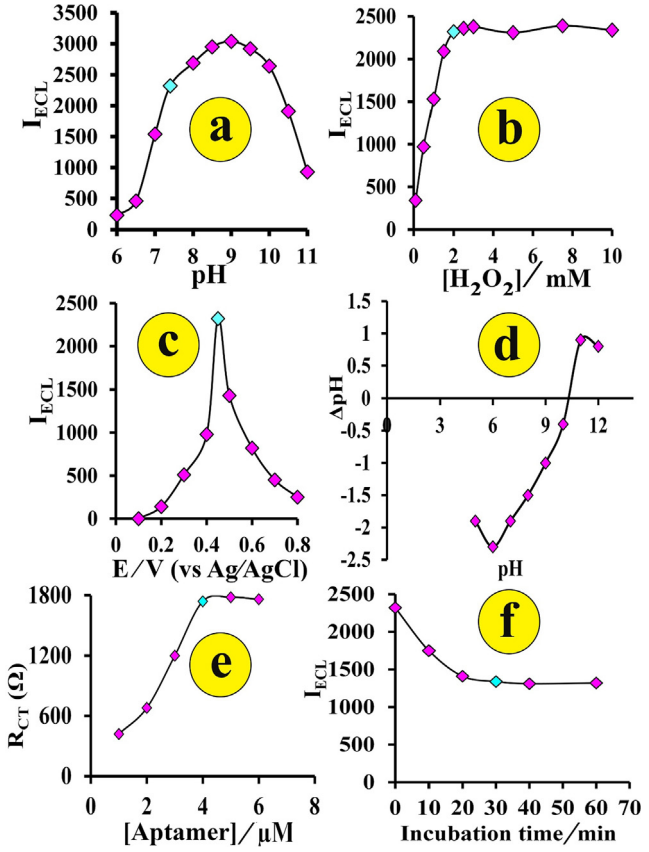

Fig. 5. Effect of the various parameters, including (a) pH (condition: 2 mM H_2O_2 and applied potential = 0.45 V), (b) H_2O_2 concentration, (c) potential effects on the ECL signal, (d) PZC of the L-Cs-Pt NPs, (e) optimization graph of aptamer concentration and (f) optimization incubation time of the aptasensor in lymphoma cells (1000 cells/mL).

the pH where ΔpH = 0 [46]. As shown in Fig. 5d, the PZC obtained for the composition of L-Cs-Pt NPs is approximately 10.3.

To optimize the concentration of immobilized aptamers, GE was treated with various aptamers concentrations from 1.0 to 6.0 μM. As shown in Fig. 5e, the R_{CT} increased with aptamer concentration up to 4.0 μM, reaching a plateau at higher aptamer concentrations. Thus, based on the EIS results, 4.0 μM was selected as the optimum concentration for the fabrication of the aptasensor. Additionally, the effect of binding time between the aptasensor and lymphoma cells on the ECL intensity was investigated (Fig. 5f). As shown in the figure, as the binding time of the GE/Ap/MCH/L-Cs-Pt NPs in PBS (pH 7.4) containing 1000 Raji cells/mL increased, the intensity of ECL (I_{ECL}) proportionally decreased by 30 min and then remained nearly constant. Therefore, 30 min was the appropriate time to obtain maximum interactions between the aptamer and target analyte.

3.6. Analytical performances of the aptasensor

The results obtained in Section 3.4 indicate that ECL peak intensities decrease in the presence of lymphoma cells. Therefore, the variation in the I_{ECL} of the aptasensor after interaction with cells at different concentrations can be used as an indicator signal for the determination of lymphoma cells. As shown in Fig. 6 (a and b), ECL intensities decreased proportionally with increasing cell concentration and were linear over the concentration range from 70 to 2090 cells/mL with a detection limit of 31 cells/mL based on $3S_d/m$ where S_d is the standard deviation of the blank measurements and m is the slope of the calibration curve [47].

The reproducibility and stability of the proposed aptasensor to detect target CD20 cells were investigated. A satisfactory RSD of 5.1% was obtained for the three aptasensors used to detect 250 cells/mL (Fig. 6c). The stability was investigated in PBS (pH = 7.4) at 4 °C over various time periods (Fig. 6d). After 14 days, a decrease of 4.2% in the ECL signal to detect the same cell counts was observed.

A comparison between the proposed method and an electrochemical immunosensor for the determination of lymphoma cells is provided in Table 2. Compared to the other biosensor in Table 2 [20], the detection limit of the proposed aptasensor is similar and the linear range is narrower than the immunosensor. The fact that the current biosensor uses an aptamer, as compared with one using an antibody, is a potential advantage because aptamers are considered to confer higher stability and reproducibility over antibodies. The proposed aptasensor is required a shorter time to determine the Raji cells (30 min) than the immunosensor (150 min). The fabrication procedure for the aptasensor is longer than for the immunosensor. The storage stability of the immunosensor and aptasensor were assessed at 7 and 14 days, respectively. The stability of the aptasensor was better in comparison. The immobilization of the recognition element is crucial in biosensors fabrication, and this is easier for aptamers than antibodies because the chemical modification of nucleic acids is simple and straightforward compared with that of antibodies [48]. Therefore, different detection schemes can be imagined in general with aptamer-based sensors as compared with antibodies. On the other hand, commercial flow cytometric assay as a reference method needs approximately 6×10^5 cells/100 μL in a final volume for test-

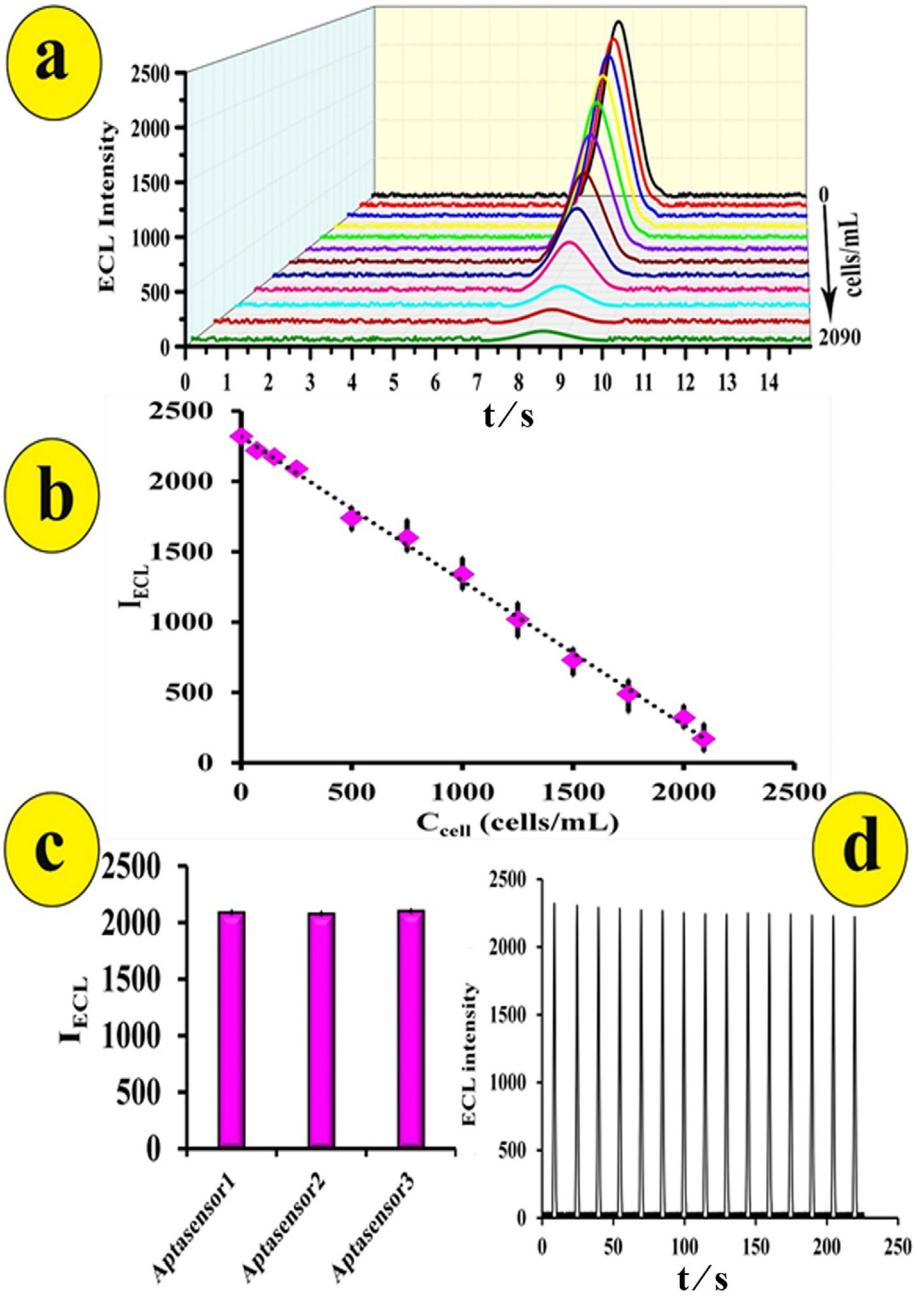

Fig. 6. (a) The ECL intensities for the incubation of the aptasensor with various CD20 cell concentrations (cells/mL), (b) its related calibration curve, (c) Reproducibility histogram of the aptasensor, and (d) ECL signal time curves of the aptasensor in PBS (pH = 7.4) at 4 °C after 14 days.

ing with antibodies. The minimum population size for quantification of cancer cells ($CD20^+$) is about 50. Indeed, the present method could detect 50 $CD20^+$ cells per 500,000 total white blood cells (WBCs) in 30–40 min. So, the level for detection of residual disease is about 0.01% the WBC population [49]. Since only these biosensors (Table 2) are described for the direct detection of Raji cells, they could be a suitable choice for application in clinical laboratories.

3.7. Control experiments

The specific adsorption of cells to the aptasensor was investigated. For this purpose, the prepared aptasensor was incubated on two different control human cells, a breast cancer cell line (MCF-7), a human embryonic kidney (HEK293), and test cells, including lymphoma cells (Raji cells). The selectivity of the aptasensor for the detection of lymphoma cells was demonstrated

Table 2
A comparison of the analytical performance of different biosensors for the determination of lymphoma cells.

Method	Bioreceptor	Concentration range (cells/mL)	Detection limit (cells/mL)	Ref.
EIS	Antibody	100–1,000,000	38	[20]
ECL	Aptamer	70–2090	31	Present work

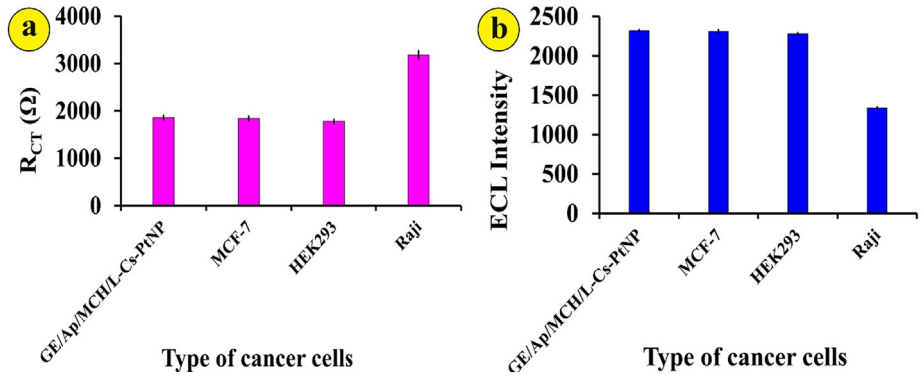

Fig. 7. (a) EIS and (b) ECL results for control experiments of aptasensor (MCF-7, HEK293, and Raji cells with the same concentration of 1000 cells/mL). The EIS experiments were performed in PBS containing 5 mM $[Fe(CN)_6]^{3-/4-}$ (1:1) and 0.1 M KCl.

by ECL and EIS measurements. After incubating the aptasensor with 1000 cells/mL concentration of control cells, only small changes in R_{CT} were observed. Incubation of the aptasensor at the same concentration of Raji cells led to an increase in the R_{CT}, demonstrating the outstanding selectivity of the sensor for lymphoma cells (Fig. 7a). By EIS observations, the ECL signal of L-Cs-Pt NPs did not change in the presence of control cells, while with Raji cells, the signal dramatically decreased (Fig. 7b).

3.8. Evaluation of L-Cs-Pt NP cytotoxicity

The viable cells were evaluated by the colorimetric MTT assay, which determines cell number based on cell proliferation [50]. Under optimal conditions, L-Cs-Pt NPs were tested by the MTT assay and did not show significant cytotoxicity. As nanoparticle concentration increased by 1–8 mg/mL, Raji cell viability exhibited no significant decrease in absorbance than the control cells. After 24 h, the MTT assay results indicated that the viability of the Raji cells was about 98% at a working concentration of 1 mg/mL of L-Cs-Pt NPs (Fig. 8). These results indicated the excellent biocompatibility of L-Cs-Pt NPs for the construction of the proposed aptasensor.

3.9. Real sample analysis

To illustrate the applicability of the proposed ECL aptasensor for the determination of Raji cells, as one example of a circulating tumor cell (CTC) in blood, [51], human blood samples were tested by the present ECL method. Raji cells were also measured in the same human blood samples using conventional flow cytometry

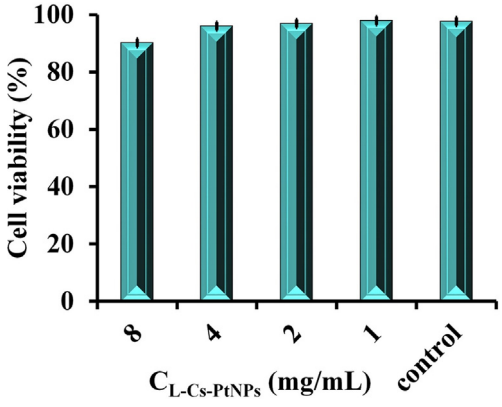

Fig. 8. Raji cell viability exposed to different concentrations of L-Cs-Pt NPs for 24 h.

Table 3
Detection of lymphoma cells in blood samples by the proposed and standard methods (N = 3).

Sample*	Found by proposed method (cells/mL)	RSD	Flow cytometry method* (cells/mL)
Blood sample 1	400	4.2	380*
Blood sample 2	500	3.9	510*

* The samples and results are the same as the ones reported in Ref. [20]. "Reprinted (adapted) with permission from [20]. Copyright (2020) American Chemical Society."

[20]. Table 3 shows the excellent correlation between the results from the two methods, confirming that the proposed strategy can be used for the satisfactory determination of circulating lymphoma cells.

4. Conclusions

A novel and sensitive method was developed for lymphoma cell direct detection at an early stage based on an ECL aptasensor, and tested on patient blood samples. Additionally, the required reagents and equipment for this purpose were simple and inexpensive. In summary, we have used the oxidation signal of accumulated L-Cs-Pt NPs on the aptasensor surface as an appropriate probe to introduce the ECL signal. With a large surface area, Cs provides a suitable matrix for Pt NP loading, and Pt NPs due to their catalytic ability dramatically enhanced the luminol ECL reaction. Therefore, ECL intensities were enhanced. The method achieved a measurment range of 70–2090 cells/mL with a low detection limit of 31 cells/mL. The satisfactory results obtained from the proposed method open a new way to applications in clinical diagnosis and real sample analysis. These results are proof-of-concept and we continue work on sandwich-type systems using both antibody and aptamer to develop high-performance devices.

Declaration of Competing Interest

The authors declare that they have no known competing financial interests or personal relationships that could have appeared to influence the work reported in this paper.

Funding

The authors would like to thank the National Institute for Medical Research Development (NIMAD) for the financial support of this work (Grant No. 982466).

Ethics approval

The project has been approved by the research ethics committee of the National Institute for Medical Research Development (NIMAD) (Approval ID: IR.NIMAD.REC.1398.126).

Appendix A. Supplementary material

Supplementary data to this article can be found online at https://doi.org/10.1016/j.bioelechem.2020.107730.

References

[1] A. Ravalli, D. Voccia, I. Palchetti, G. Marrazza, Electrochemical, electrochemiluminescence, and photoelectrochemical aptamer-based nanostructured sensors for biomarker analysis, Biosensors 6 (3) (2016) 39.

[2] Y.N. Khonsari, S. Sun, Recent trends in electrochemiluminescence aptasensors and their applications, Chem. Commun. 53 (65) (2017) 9042–9054.

[3] S.A. Kitte, W. Gao, Y.T. Zholudov, L. Qi, A. Nsabimana, Z. Liu, G. Xu, Stainless steel electrode for sensitive luminol electrochemiluminescent detection of H2O2, glucose, and glucose oxidase activity, Anal. Chem. 89 (18) (2017) 9864–9869.

[4] R. Poorghasem, R.S. Saberi, M. Shayan, M.A. Mehrgardi, A. Kiani, Closed bipolar electrochemistry for the detection of human immunodeficiency virus short oligonucleotide, Electrochim. Acta 222 (2016) 1483–1490.

[5] X.-B. Yin, Y.-Y. Xin, Y. Zhao, Label-free electrochemiluminescent aptasensor with attomolar mass detection limits based on a Ru (phen) 32+-double-strand DNA composite film electrode, Anal. Chem. 81 (22) (2009) 9299–9305.

[6] G. Jie, Y. Zhao, S. Niu, Amplified electrochemiluminescence detection of cancer cells using a new bifunctional quantum dot as signal probe, Biosens. Bioelectron. 50 (2013) 368–372.

[7] J.-J. Zhang, J.-T. Cao, G.-F. Shi, K.-J. Huang, Y.-M. Liu, Y.-H. Chen, Label-free and sensitive electrochemiluminescence aptasensor for the determination of 17β-estradiol based on a competitive assay with cDNA amplification, Anal. Methods 6 (17) (2014) 6796–6801.

[8] C. Ding, S. Wei, H. Liu, Electrochemiluminescent determination of cancer cells based on aptamers, nanoparticles, and magnetic beads, Chem. Eur. J. 18 (23) (2012) 7263–7268.

[9] Y. Sheng, H. Yang, Y. Wang, L. Han, Y. Zhao, A. Fan, Silver nanoclusters-catalyzed luminol chemiluminescence for hydrogen peroxide and uric acid detection, Talanta 166 (2017) 268–274.

[10] S.M. Khoshfetrat, M. Ranjbari, M. Shayan, M.A. Mehrgardi, A. Kiani, Wireless electrochemiluminescence bipolar electrode array for visualized genotyping of single nucleotide polymorphism, Anal. Chem. 87 (16) (2015) 8123–8131.

[11] W. Lian, S. Liu, J. Yu, X. Xing, J. Li, M. Cui, J. Huang, Electrochemical sensor based on gold nanoparticles fabricated molecularly imprinted polymer film at chitosan–platinum nanoparticles/graphene–gold nanoparticles double nanocomposites modified electrode for detection of erythromycin, Biosens. Bioelectron. 38 (1) (2012) 163–169.

[12] M.J. Laudenslager, J.D. Schiffman, C.L. Schauer, Carboxymethyl chitosan as a matrix material for platinum, gold, and silver nanoparticles, Biomacromolecules 9 (10) (2008) 2682–2685.

[13] M. Madkour, A. Bumajdad, F. Al-Sagheer, To what extent do polymeric stabilizers affect nanoparticles characteristics?, Adv. Colloid Interface Sci. 270 (2019) 38–53.

[14] S. Pothukuchi, Y. Li, C. Wong, Shape controlled synthesis of nanoparticles and their incorporation into polymers, in: 2004 Proceedings. 54th Electronic Components and Technology Conference (IEEE Cat. No. 04CH37546), IEEE, 2004, 1965-–1967.

[15] M. Adlim, M.A. Bakar, K.Y. Liew, J. Ismail, Synthesis of chitosan-stabilized platinum and palladium nanoparticles and their hydrogenation activity, J. Mol. Catal. A: Chem. 212 (1–2) (2004) 141–149.

[16] L. Wang, Q. Xiong, F. Xiao, H. Duan, 2D nanomaterials based electrochemical biosensors for cancer diagnosis, Biosens. Bioelectron. 89 (2017) 136–151.

[17] C. Ding, Y. Ge, S. Zhang, Electrochemical and electrochemiluminescence determination of cancer cells based on aptamers and magnetic beads, Chem. Eur. J. 16 (35) (2010) 10707–10714.

[18] J. Lin, H. Ju, Electrochemical and chemiluminescent immunosensors for tumor markers, Biosens. Bioelectron. 20 (8) (2005) 1461–1470.

[19] L. Tan, P. Lin, M.M. Chisti, A. Rehman, X. Zeng, Real time analysis of binding between Rituximab (anti-CD20 antibody) and B lymphoma cells, Anal. Chem. 85 (18) (2013) 8543–8551.

[20] P. Hashemi, A. Afkhami, B. Baradaran, R. Halabian, T. Madrakian, F. Arduini, T.-A. Nguyen, H. Bagheri, Well-orientation strategy for direct immobilization of antibodies: development of the immunosensor using the boronic acid-modified magnetic graphene nanoribbons for ultrasensitive detection of lymphoma cancer cells, Anal. Chem. 92 (16) (2020) 11405–11412.

[21] J. Wu, Z. Fu, F. Yan, H. Ju, Biomedical and clinical applications of immunoassays and immunosensors for tumor markers, TrAC, Trends Anal. Chem. 26 (7) (2007) 679–688.

[22] M. Sözmen, S. Tasca, E. Carli, D.D. Lorenzi, T. Furlanello, M. Caldin, Use of fine needle aspirates and flow cytometry for the diagnosis, classification, and immunophenotyping of canine lymphomas, J. Vet. Diagn. Invest. 17 (4) (2005) 323–329.

[23] M.G. Ribeiro, L.A. Neves, G.F. Roberto, T.A. Tosta, A.S. Martins, M.Z. Do Nascimento, Analysis of the influence of color normalization in the classification of non-Hodgkin Lymphoma images, in: Proceedings of the 31st SIBGRAPI conference on graphics, patterns and images (SIBGRAPI), IEEE (2018) 369–376.

[24] A. Khanmohammadi, A. Aghaie, E. Vahedi, A. Qazvini, M. Ghanei, A. Afkhami, A. Hajian, H. Bagheri, Electrochemical biosensors for the detection of lung cancer biomarkers: a review, Talanta 206 (2020) 120251.

[25] M.M. Richter, Electrochemiluminescence (ecl), Chem. Rev. 104 (6) (2004) 3003–3036.

[26] S. Huang, R. Tang, T. Zhang, J. Zhao, Z. Jiang, Q. Wang, Anti-fouling poly adenine coating combined with highly specific CD20 epitope mimetic peptide for rituximab detection in clinical patients' plasma, Biosens. Bioelectron. 171 (2021) 112678.

[27] P.R. Mallikaratchy, A. Ruggiero, J.R. Gardner, V. Kuryavyi, W.F. Maguire, M.L. Heaney, M.R. McDevitt, D.J. Patel, D.A. Scheinberg, A multivalent DNA aptamer specific for the B-cell receptor on human lymphoma and leukemia, Nucl. Acids Res. 39 (6) (2011) 2458–2469.

[28] A. Kiani, E.N. Fard, Fabrication of palladium coated nanoporous gold film electrode via underpotential deposition and spontaneous metal replacement: a low palladium loading electrode with electrocatalytic activity, Electrochim. Acta 54 (28) (2009) 7254–7259.

[29] M.A. Mehrgardi, L.E. Ahangar, Silver nanoparticles as redox reporters for the amplified electrochemical detection of the single base mismatches, Biosens. Bioelectron. 26 (11) (2011) 4308–4313.

[30] L. Feng, Y. Chen, J. Ren, X. Qu, A graphene functionalized electrochemical aptasensor for selective label-free detection of cancer cells, Biomaterials 32 (11) (2011) 2930–2937.

[31] A.C. Seegmiller, E.D. Hsi, F.E. Craig, The current role of clinical flow cytometry in the evaluation of mature B-cell neoplasms, Cytometry, Part B 96 (1) (2019) 20–29.

[32] K. Esumi, A. Suzuki, A. Yamahira, K. Torigoe, Role of poly (amidoamine) dendrimers for preparing nanoparticles of gold, platinum, and silver, Langmuir 16 (6) (2000) 2604–2608.

[33] E. Nalewajko, R.B. Ramírez, A. Kojło, Determination of dopamine by flow-injection analysis coupled with luminol-hexacyanoferrate (III) chemiluminescence detection, J. Pharm. Biomed. Anal. 36 (1) (2004) 219–223.

[34] A. Afkhami, P. Hashemi, H. Bagheri, J. Salimian, A. Ahmadi, T. Madrakian, Impedimetric immunosensor for the label-free and direct detection of botulinum neurotoxin serotype A using Au nanoparticles/graphene-chitosan composite, Biosens. Bioelectron. 93 (2017) 124–131.

[35] S. Chen, P. Fu, B. Yin, R. Yuan, Y. Chai, Y. Xiang, Immobilizing Pt nanoparticles and chitosan hybrid film on polyaniline nanofibers membrane for an amperometric hydrogen peroxide biosensor, Bioprocess Biosyst. Eng. 34 (6) (2011) 711–719.

[36] A. Wroblewska, O. Reshetnyak, E. Koval'chuk, R. Pasichnyuk, J. Błażejowski, Origin and features of the electrochemiluminescence of luminol–experimental and theoretical investigations, J. Electroanal. Chem. 580 (1) (2005) 41–49.

[37] G. Yildiz, U. Tasdoven, N. Menek, Electrochemical characterization of luminol and its determination in real samples, Anal. Methods 6 (19) (2014) 7809–7813.

[38] J. Liang, M. Li, Y. Lu, H. Yao, H. Liu, An enzymatic calculation system based on electrochemiluminescence and fluorescence of luminol and cyclic voltammetry of ferrocene methanol, Biosens. Bioelectron. 118 (2018) 44–50.

[39] S. Campuzano, M. Pedrero, C. Montemayor, E. Fatás, J.M. Pingarrón, Characterization of alkanethiol-self-assembled monolayers-modified gold electrodes by electrochemical impedance spectroscopy, J. Electroanal. Chem. 586 (1) (2006) 112–121.

[40] C. Pan, M. Guo, Z. Nie, X. Xiao, S. Yao, Aptamer-based electrochemical sensor for label-free recognition and detection of cancer cells, Electroanal. Int. J. Fundam. Pract. Aspects Electroanal. 21 (11) (2009) 1321–1326.

[41] B. Hinnemann, J.K. Nørskov, H. Topsøe, A density functional study of the chemical differences between type I and type II MoS2-based structures in hydrotreating catalysts, J. Phys. Chem. B 109 (6) (2005) 2245–2253.

[42] M.R.K. Pur, M. Hosseini, F. Faridbod, M.R. Ganjali, Highly sensitive label-free electrochemiluminescence aptasensor for early detection of myoglobin, a biomarker for myocardial infarction, Microchim. Acta 184 (9) (2017) 3529–3537.

[43] S.-G. Wang, X.-F. Sun, X.-W. Liu, W.-X. Gong, B.-Y. Gao, N. Bao, Chitosan hydrogel beads for fulvic acid adsorption: Behaviors and mechanisms, Chem. Eng. J. 142 (3) (2008) 239–247.

[44] J. Maity, S.K. Ray, Enhanced adsorption of methyl violet and congo red by using semi and full IPN of polymethacrylic acid and chitosan, Carbohydr. Polym. 104 (2014) 8–16.

[45] N. Hao, X. Zhang, Z. Zhou, R. Hua, Y. Zhang, Q. Liu, J. Qian, H. Li, K. Wang, AgBr nanoparticles/3D nitrogen-doped graphene hydrogel for fabricating all-solid-state luminol-electrochemiluminescence Escherichia coli aptasensors, Biosens. Bioelectron. 97 (2017) 377–383.

[46] H. Bagheri, A. Afkhami, M. Saber-Tehrani, H. Khoshsafar, Preparation and characterization of magnetic nanocomposite of Schiff base/silica/magnetite as a preconcentration phase for the trace determination of heavy metal ions in water, food and biological samples using atomic absorption spectrometry, Talanta 97 (2012) 87–95.

[47] G.L. Long, J.D. Winefordner, Limit of detection. A closer look at the IUPAC definition, Anal. Chem. 55 (7) (1983) 712A–724A.
[48] J.-O. Lee, H.-M. So, E.-K. Jeon, H. Chang, K. Won, Y.H. Kim, Aptamers as molecular recognition elements for electrical nanobiosensors, Anal. Bioanal. Chem. 390 (4) (2008) 1023–1032.
[49] A.K. Dowling, S.D. Liptrot, D. O'Brien, E. Vandenberghe, Optimization and validation of an 8-color single-tube assay for the sensitive detection of minimal residual disease in b-cell chronic lymphocytic leukemia detected via flow cytometry, Lab. Med. 47 (2) (2016) 103–111.
[50] L. Kashefi-Kheyrabadi, M.A. Mehrgardi, E. Wiechec, A.P. Turner, A. Tiwari, Ultrasensitive detection of human liver hepatocellular carcinoma cells using a label-free aptasensor, Anal. Chem. 86 (10) (2014) 4956–4960.
[51] A.A. Adams, P.I. Okagbare, J. Feng, M.L. Hupert, D. Patterson, J. Göttert, R.L. McCarley, D. Nikitopoulos, M.C. Murphy, S.A. Soper, Highly efficient circulating tumor cell isolation from whole blood and label-free enumeration using polymer-based microfluidics with an integrated conductivity sensor, J. Am. Chem. Soc. 130 (27) (2008) 8633–8641.